Electronic Supplementary Information

A high-performance rocking-chair lithium-ion battery-supercapacitor hybrid device boosted by doubly matched capacity and kinetics of faradaic Electrodes

Feng Su,[ab] Jieqiong Qin,[ad] Pratteek Das,[ab] Feng Zhou,[ac] and Zhong-Shuai Wu*[ac]

[a] State Key Laboratory of Catalysis, Dalian Institute of Chemical Physics, Chinese Academy of Sciences, 457 Zhongshan Road, Dalian 116023, China. E-mail: wuzs@dicp.ac.cn

[b] University of Chinese Academy of Sciences, 19 A Yuquan Rd, Shijingshan District, Beijing 100049, China

[c] Dalian National Laboratory for Clean Energy, Chinese Academy of Sciences, 457 Zhongshan Road, Dalian 116023, China

[d] College of Science, Henan Agricultural University, No. 63 Agricultural Road, Zhengzhou 450002, China

Experimental

Synthesis of T-Nb_2O_5 nanoflowers

80 mg niobium oxalate were dissolved in 28 mL deionized water and 12 mL ethylene glycol to form homogenous solution. Then, $NH_3 \cdot H_2O$ solution was slowly added into the mixture until the pH reached 9. The reaction mixture was transferred and sealed in a 50 mL Teflon-lined stainless autoclave and kept at 150 ^oC for 24 h. The resulting white precipitate was collected by centrifugation and washed with deionized water three times, followed by freeze-drying. After calcination at 650 ^oC in air for 3 h with a heating rate of 1 ^oC min^{-1}, T-Nb_2O_5 nanoflowers were obtained.

Electrode fabrication

T-Nb_2O_5-NF electrodes were prepared by mixing the active material, acetylene black and poly(vinylidene fluoride) at a mass ratio of 8:1:1 in N-methyl pyrrolidone solvent to form a uniform slurry, which was then coated on carbon-coated Al foil.

Graphene sheets were prepared by an electrochemically cathodic exfoliation method, as described previously.[1] To fabricate NCA-3D electrodes, the electrochemically exfoliated graphene (EG) sheets and multi-walled carbon nanotubes (CNTs, diameter: 10−20 nm; length: 5−15 μm; Aladin) were first dispersed in absolute ethanol by sonication for 2 h. Afterwards, $LiNi_{0.815}Co_{0.15}Al_{0.035}O_2$ (NCA) microspheres (MTI corporation) were added and further sonicated for 30 min. The mixture was filtered and dried in vacuum oven at 80 ^oC. The dried products were mixed with poly(3-hexylthiophene-2,5-diyl) (P3HT) conductive polymer binder in o-dichlorobenzene solvent and then coated on carbon-coated Al foil. The mass ratio of NCA, EG, CNTs and P3HT was 90:4:3:3. For comparison, conventional NCA-C electrodes were prepared by a doctor-blading process using 7% acetylene black and 3% poly(vinylidene fluoride) as conductive additive and binder. All the electrodes were dried in vacuum oven at 100 ^oC overnight. The mass loading of active materials was 1.2~2 mg cm^{-2}.

Material characterization

The morphology, composition, and structure of materials were characterized by field emission scanning electron microscopy (JSM-7800F), transition electron microscopy (JEM-2100), X-ray powder diffraction (X'Pert Pro with Cu Kα radiation, 0.15406 nm) and Raman spectrometer (Bruker Optics Senterra, 532 nm).

Cell assembly and electrochemical measurement

For half-cell tests, CR2016-type coin cells were assembled in an argon-filled glovebox with H_2O and O_2 concentration below 1 ppm, using lithium metal as both counter and reference electrodes, and polypropylene membrane (Celgard 2500) as separator, together with electrolyte composed of 1 M $LiPF_6$ in ethylene carbonate / dimethyl carbonate / diethyl carbonate (1:1:1, volume ratio). The full cells were constructed using T-Nb_2O_5-NF as anode and NCA-3D or NCA-C as cathode in CR2016-type coin cell.

Galvanostatic charge and discharge (GCD) measurements were performed on a LAND CT2001A battery test system for half cells, and an electrochemical workstation (CHI 760E) for the full cells. Cyclic voltammetry (CV) was conducted on CHI 760E. Electrochemical impedance spectroscopy (EIS) was measured by CHI 760E in the frequency range of 100 kHz to 0.01 Hz with an amplitude of 5 mV. Before EIS test, the electrodes were held at certain potential for 2 h to obtain a state of equilibrium.

The capacities were evaluated based on the mass of active materials in the electrodes. The energy density (E, Wh kg^{-1}) and average power density (P, W kg^{-1}) were calculated from GCD curves using the following equations:

$$E = \int_0^t \frac{VI}{3600m} dt$$

$$P = \frac{E}{t} \times 3600$$

where V is the voltage of the full cell (V), I is the discharge current (A), m is the total mass of active materials in both anode and cathode (kg) and t is the discharge time (s), respectively.

The average discharge voltage of the full cell was calculated *via* dividing energy density by capacity:

$$V_{average} = \frac{\int_0^t \frac{VI}{3600m} dt}{It}$$

Three-electrode GCD measurement was conducted using a home-made three-electrode cell with two stainless steel plungers and a silver wire quasi-reference electrode (Fig. S13). The two working electrodes were separated by two sheets of glass fiber separator, and the silver wire reference electrode was placed between the two layers of separators.

To check the reproducibility of the proposed system, several parallel experiments were carried out using electrodes from different batches, and at least three cells with almost identical electrochemical performance were used to confirm the reproducibility.

Supplementary Note: Calculation details for the theoretical energy density based on active material and electrolyte

Estimating the theoretical energy density of the electrolyte-consuming BSHD (BNC//BNC)

In the case of electrolyte-consuming cells, the required minimum amount of electrolyte is estimated from the charge balance relationship of $Q_d = Q_i$, where Q_d is the charge stored in the electrode, Q_i is the charge of the ions consumed from electrolyte.[2] A BSHD based on B and N dual-doped carbon nanofibers (BNC//BNC) is used as an example for calculation, which exhibits an energy density of 220 Wh kg^{-1} based on the mass of active material with the voltage range of 0−4.5 V and cathode:anode mass ratio of 3 in the electrolyte composed of 1 M $LiPF_6$ in ethylene carbonate and diethyl carbonate with a volume ratio of 1:1.[3]

(1) Considering the anode is prelithiated, the capacity of the cathode is used to calculate the required charge from electrolyte. Assuming the cathode works with electrolyte-consuming mechanism in the potential window of 3−4.5 V *vs.* Li^+/Li (since the open-circuit voltage of carbon-based material in $LiFP_6$-based electrolyte is approximately 3 V *vs.* Li^+/Li [4] and the maximum voltage of the full cell is 4.5 V), the corresponding capacity is ~68 mAh g^{-1}, according to the GCD profiles of the cathode.

The mass ratio of cathode and anode is 3:1. Then, the corresponding capacity based on the mass of active materials in both cathode and anode is:

$$\frac{68 \times 3}{1+3} = 51\ mAh\ g^{-1}$$

(2) The required volume of the 1 M $LiPF_6$ electrolyte is:

$$V_i = \frac{Q_d}{Fc_i}$$

where F = 96484 C mol^{-1} is Faraday's constant, c_i is the molar concentration of the electrolyte.

The mass of active materials is set to 1 g for simplicity, then Q_d = 51 mAh = 183.6 C. The required volume of the electrolyte is:

$$V_i = \frac{183.6}{96484 \times 1} \times 1000 = 1.9\ cm^3$$

(3) The mass density of the used electrolyte (ρ_i) is 1.2 g cm^{-3}.[5] Then the mass ratio of the electrolyte and active materials is:

$$\alpha = \frac{\rho_i V_i}{1} = 2.28$$

(4) The energy density based on the active materials and electrolyte is:

$$E = \frac{220}{1 + 2.28} = 67\ Wh\ kg^{-1}$$

It should be noted that a large excess of electrolyte is still needed for maintaining ionic conductivity upon charge in practical devices.[2] Therefore, the actual energy density at device level may be much lower than this theoretical value.

Estimating the theoretical energy density of the rocking-chair BSHD (T-Nb_2O_5-NF//NCA-3D)

In the case of rocking-chair cells, the required minimum amount of electrolyte is estimated according to the pore volume of the electrodes, which must be filled by electrolyte to provide sufficient ionic conductive path.[6] The energy density based on the mass of active materials and the minimum amount of electrolyte is calculated as follows:

(1) The electrode porosity is:

$$p = \frac{\rho_t - \rho_m}{\rho_t}$$

where ρ_t is the true density of electrode materials, ρ_m is electrode mass density.

(1.1) ρ_t for Nb_2O_5, NCA, carbon material, PVDF and P3HT is 4.5 g cm^{-3}, 4.8 g cm^{-3}, 2.2 g cm^{-3}, 1.8 g cm^{-3} and 1.0 g cm^{-3}, respectively.[5,7] The mass of anode and cathode is set to 1 g for simplicity. Then, the true density of the whole electrode is:

$$\rho_t(anode) = \frac{1}{\frac{0.8}{4.5} + \frac{0.1}{2.2} + \frac{0.1}{1.8}} = 3.59\ g\ cm^{-3}$$

$$\rho_t(cathode) = \frac{1}{\frac{0.9}{4.8} + \frac{0.07}{2.2} + \frac{0.03}{1.0}} = 4.01\ g\ cm^{-3}$$

(1.2) The electrode mass density is:

$$\rho_m(anode) = \frac{m_a}{L_a} = \frac{1.75 \times 10^{-3}}{19 \times 10^{-4}} = 0.92\ g\ cm^{-3}$$

$$\rho_m(cathode) = \frac{m_c}{L_c} = \frac{1.58 \times 10^{-3}}{15 \times 10^{-4}} = 1.05\ g\ cm^{-3}$$

where m is the total mass loading of the electrodes, L is the thickness of the electrodes, which is 19 μm for the anode with a total mass loading of 1.75 mg cm^{-2} and 15 μm for the cathode with a total mass loading of 1.58 mg cm^{-2} according to Fig. S23.

(1.3) The electrode porosity is:

$$p_a = \frac{3.59 - 0.92}{3.59} = 74\%$$

$$p_c = \frac{4.01 - 1.05}{4.01} = 74\%$$

(2) The pore volume of the anode and cathode is:

$$V_a = \frac{m_a}{\rho_m(anode)} p_a = \frac{1.75 \times 10^{-3}}{0.92} \times 74\% = 0.0014\ cm^{-3}$$

$$V_c = \frac{m_c}{\rho_m(cathode)} p_c = \frac{1.58 \times 10^{-3}}{1.05} \times 74\% = 0.0011\ cm^{-3}$$

(3) The mass density of the electrolyte (ρ_i) is 1.2 g cm^{-3}. Then, the mass of the required electrolyte is:

$$m_i = \rho_i(V_a + V_c) = 1.2 \times (0.0014 + 0.0011) \times 10^3 = 3\ mg$$

(4) The mass ratio of electrolyte and active materials is:

$$\alpha = \frac{3}{1.75 \times 0.8 + 1.58 \times 0.9} = 1.06$$

(5) The energy density based on the active materials and electrolyte is:

$$E = \frac{165}{1 + 1.06} = 80\ Wh\ kg^{-1}$$

It should be noted that this energy density could be further improved by optimizing the density of the electrodes since no compaction process is applied in this work. The above results reveal that the theoretical energy density of the rocking-chair BSHD in this work is comparable and even superior to those of the state-of-the-art electrolyte-consuming BSHDs, demonstrative of the superiority of rocking-chair configuration.

Supplementary Figures

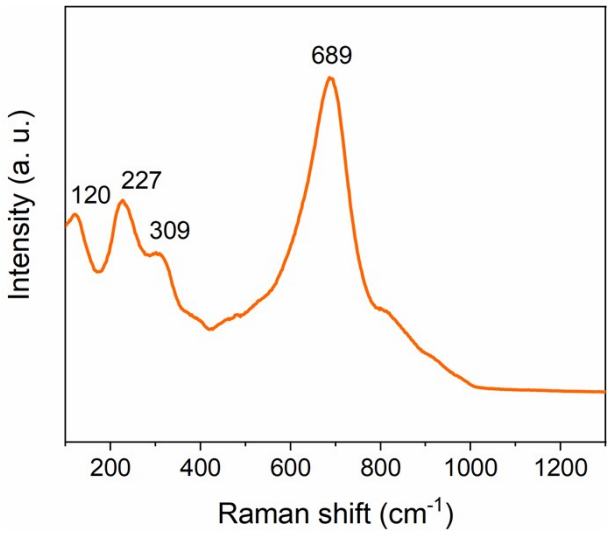

Fig. S1 Raman spectrum of T-Nb_2O_5-NF.

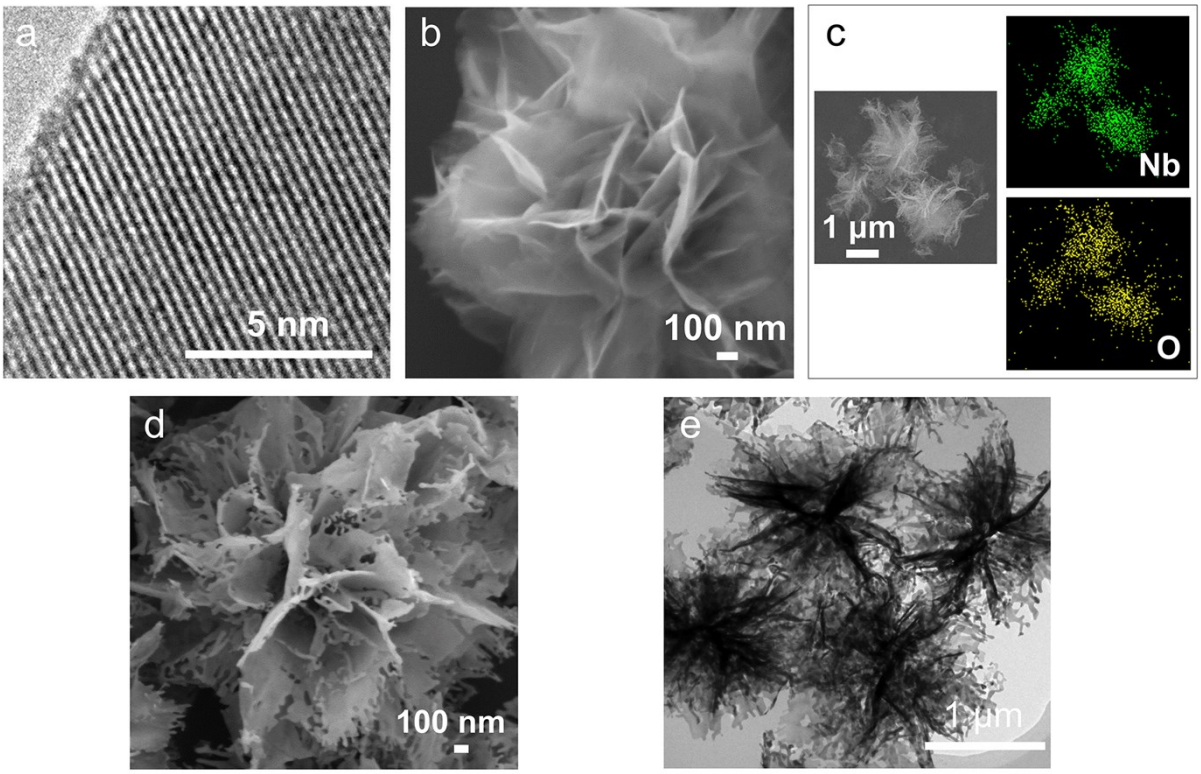

Fig. S2 (a) HRTEM image of T-Nb_2O_5-NF. (b) SEM image of Nb_2O_5 nanoflower before calcination. (c) EDS elemental mapping, (d) SEM and (e) TEM images of T-Nb_2O_5-NF.

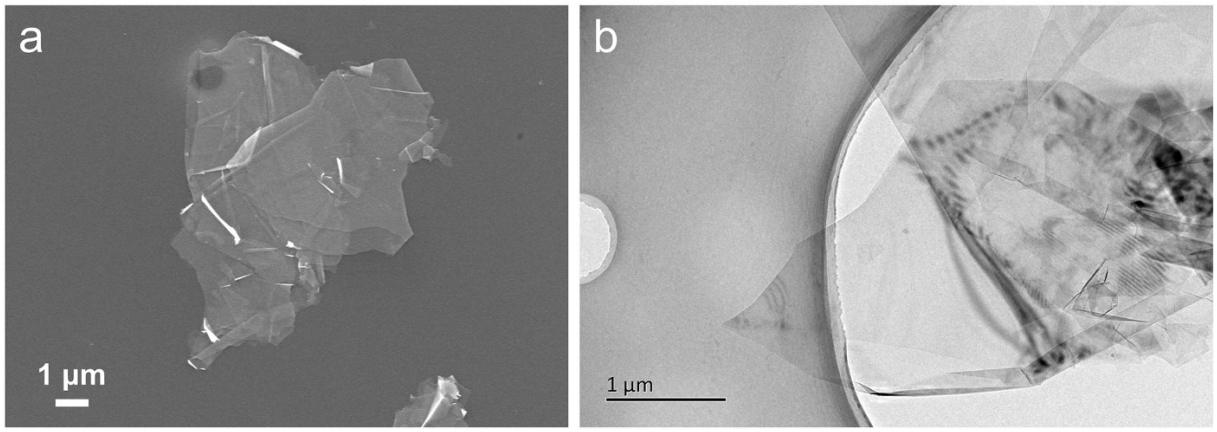

Fig. S3 (a) SEM and (b) TEM images of EG sheets.

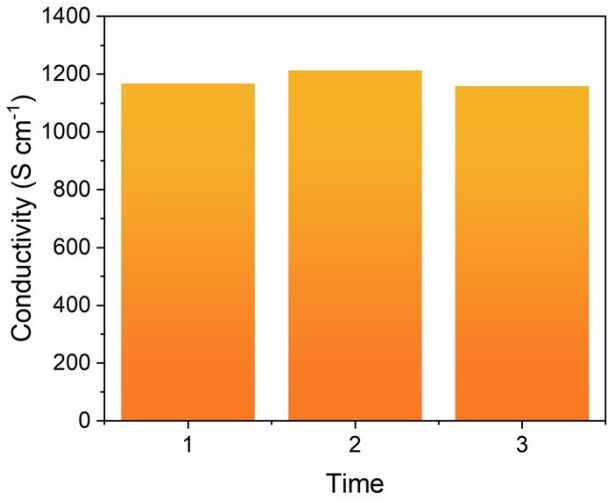

Fig. S4 Electrical conductivity of EG thin film with a thickness of ~1.9 μm. The measurement was performed on a four-point probe equipment (RTS-9).

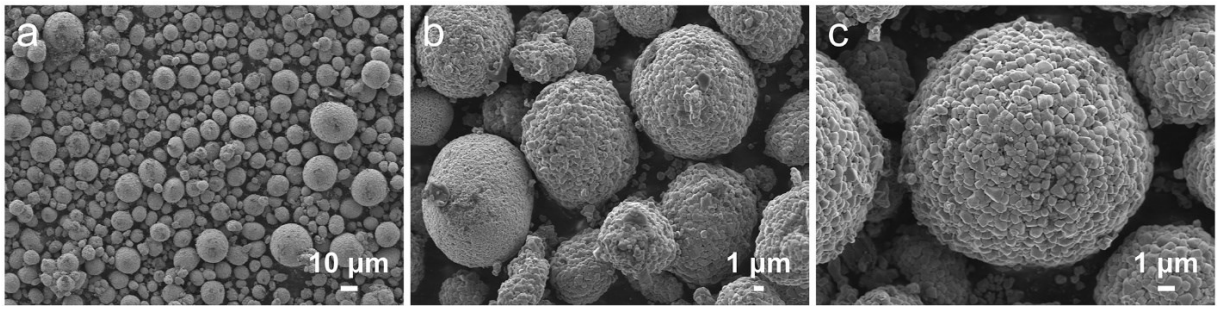

Fig. S5 SEM images of pristine NCA under different magnifications.

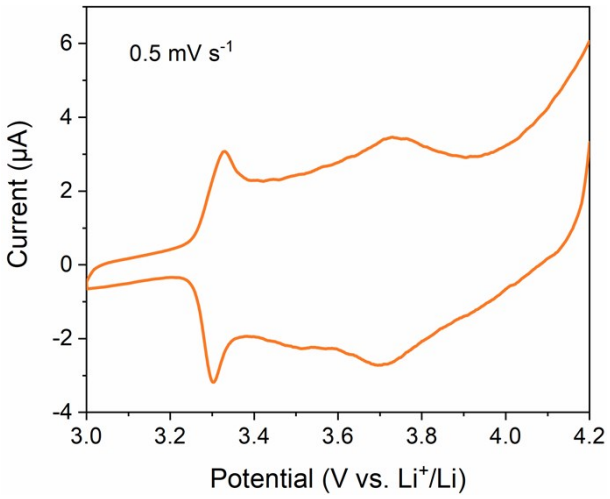

Fig. S6 CV curve of P3HT at a scan rate of 0.5 mV s^{-1}. The electrodes were prepared by mixing P3HT with CNT at a mass ratio of 1:1.

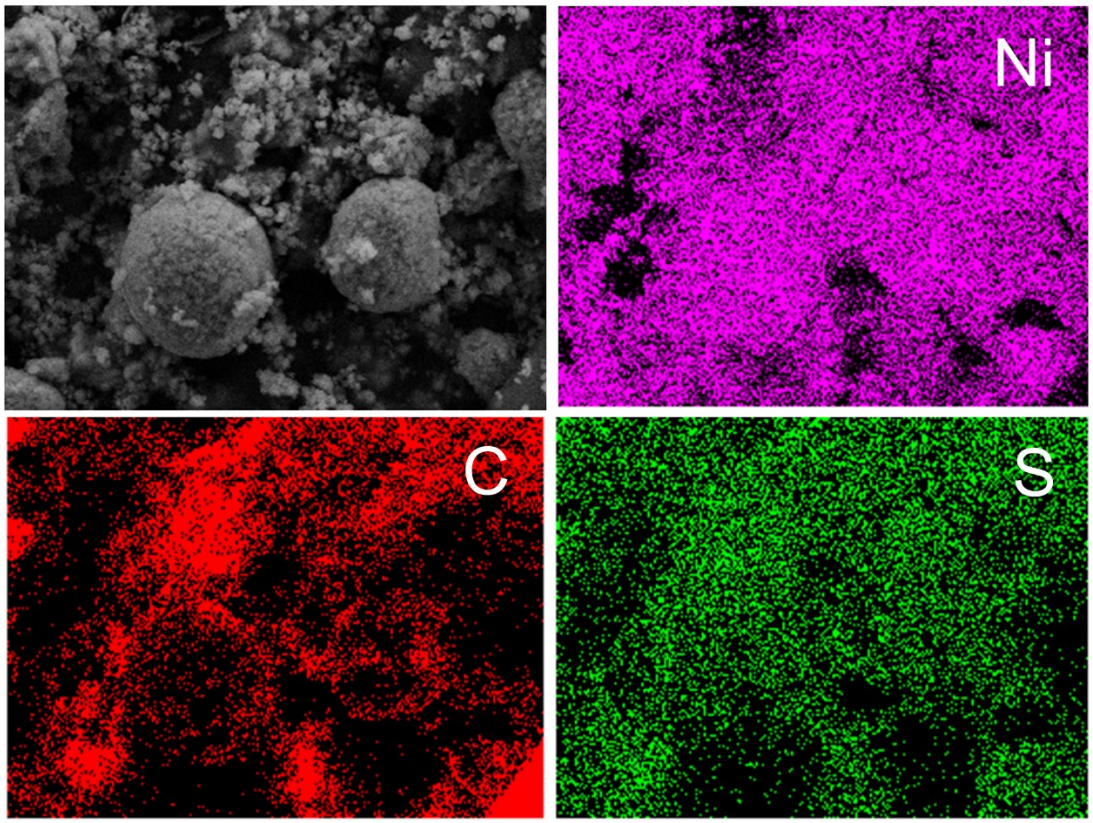

Fig. S7 EDS elemental mapping images of NCA-3D electrode. The mapping of Ni, C, S elements are used to represent the existence of NCA, CNT/EG and P3HT, respectively.

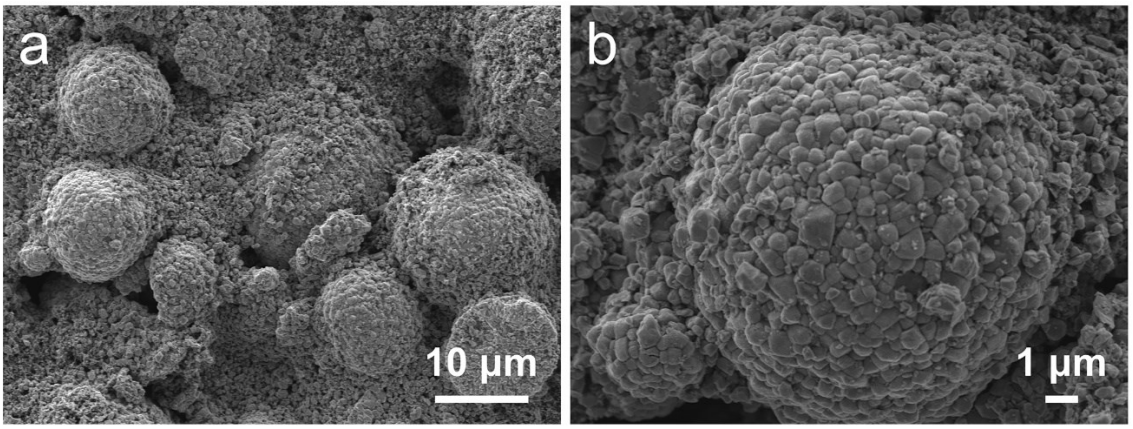

Fig. S8 SEM images of NCA-C electrode under different magnifications.

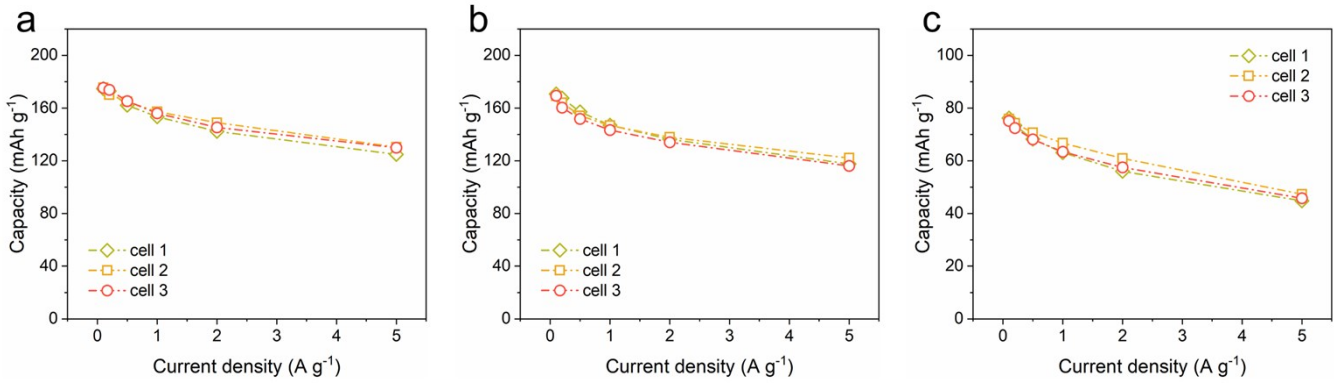

Fig S9 Capacity as a function of current density for three individual (a) Li//T-Nb_2O_5-NF half cells, (b) Li//NCA-3D half cells and (c) T-Nb_2O_5-NF//NCA-3D full cells.

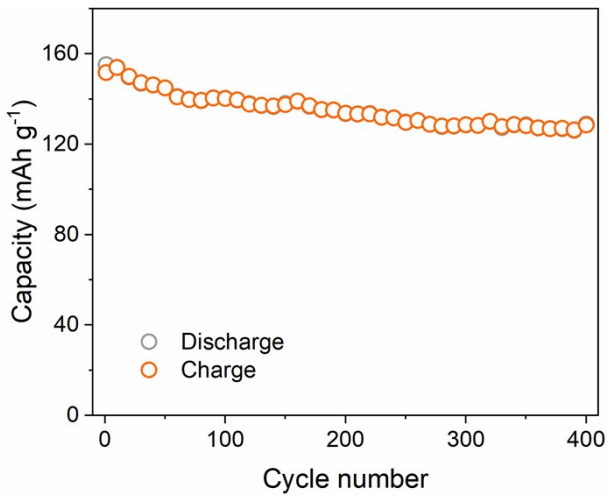

Fig. S10 Cycling stability of T-Nb_2O_5-NF measured at a current density of 1 A g^{-1}.

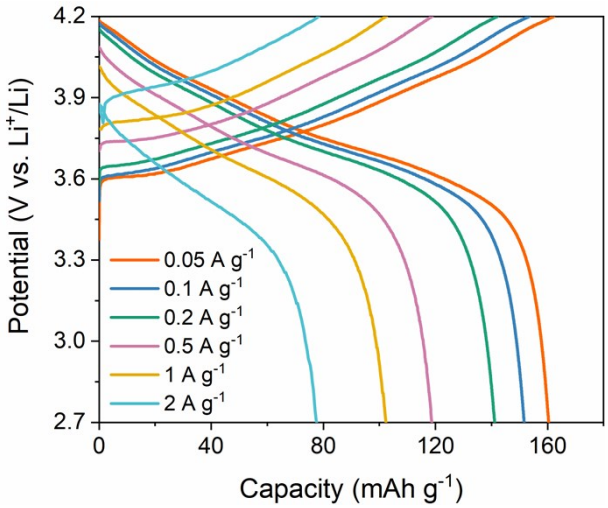

Fig. S11 GCD profiles of NCA-C electrodes tested at current densities from 0.05 to 5 A g^{-1}.

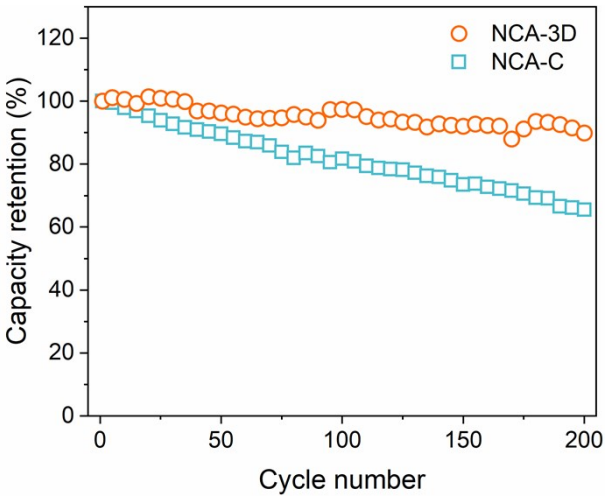

Fig. S12 Cycling performance of NCA-3D and NCA-C electrodes tested at 1 A g^{-1} after measuring rate capability.

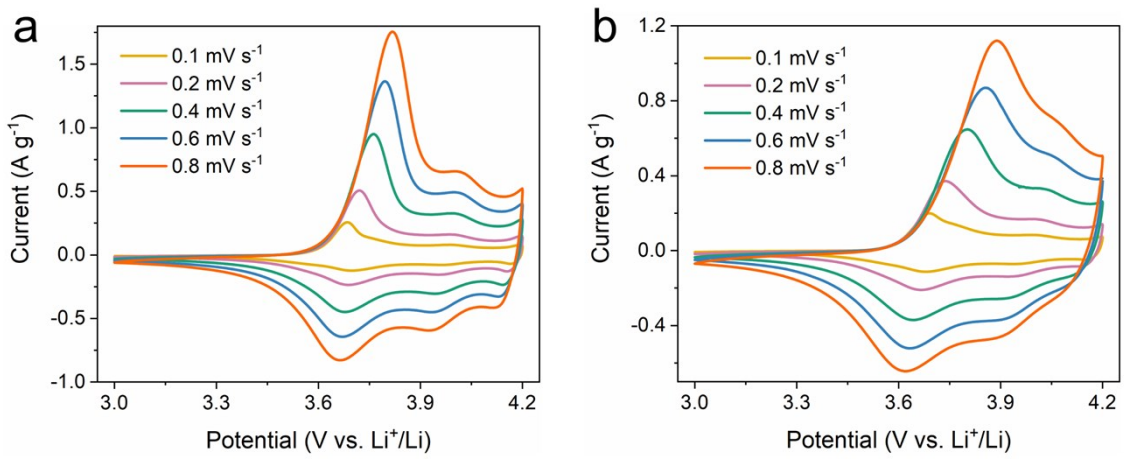

Fig. S13 CV curves of (a) NCA-3D and (b) NCA-C electrodes measured at sweep rates from 0.1 to 0.8 mV s^{-1}.

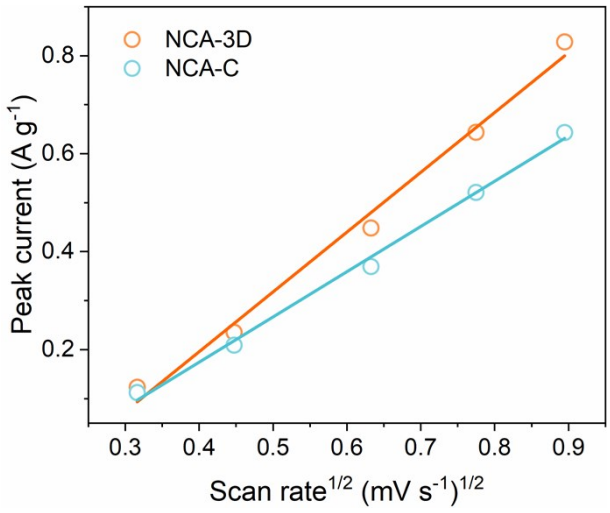

Fig. S14 Cathodic peak current as a function of sweep $rate^{1/2}$ for NCA-3D and NCA-C electrodes.

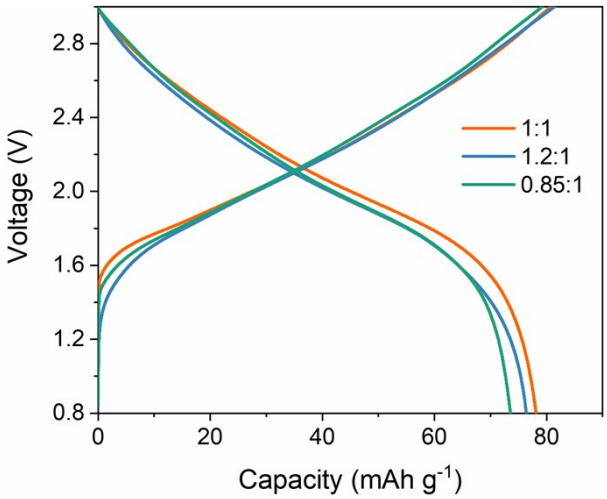

Fig. S15 GCD profiles of T-Nb_2O_5-NF//NCA-3D BSHDs with different mass ratios between cathode and anode at a current density of 0.05 A g^{-1}.

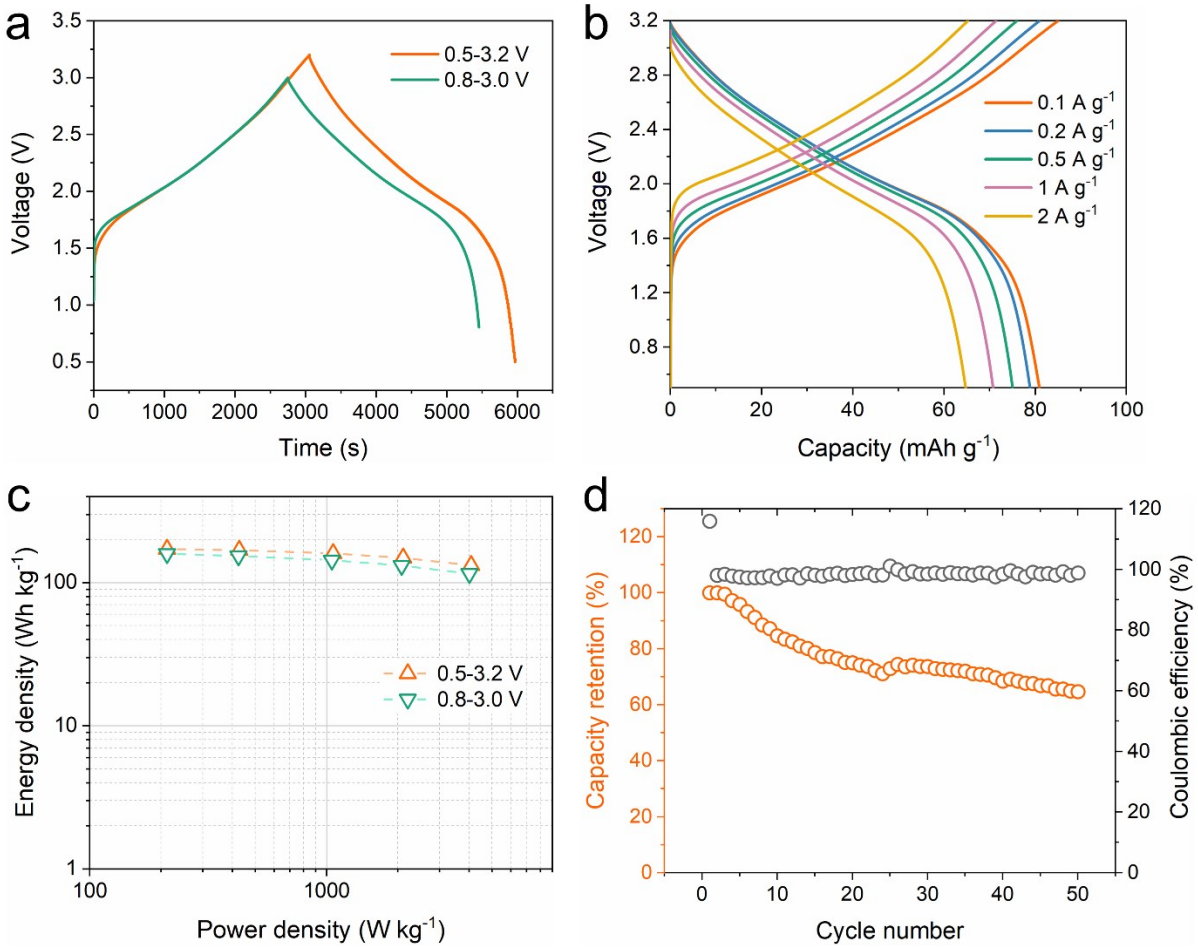

Fig. S16 (a) GCD profiles of T-Nb_2O_5-NF//NCA-3D BSHDs obtained at 0.1 A g^{-1} within different voltage windows. (b) GCD profiles of T-Nb_2O_5-NF//NCA-3D BSHDs measured at various current densities within the voltage range of 0.5–3.2 V. (c) Ragone plots of T-Nb_2O_5-NF//NCA-3D BSHDs within different voltage windows. (d) Cycling stability and Coulombic efficiency of T-Nb_2O_5-NF//NCA-3D BSHDs tested at 1 A g^{-1} within the voltage range of 0.5–3.2 V.

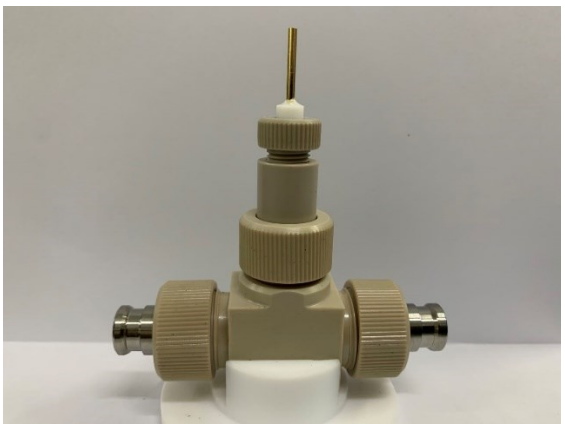

Fig. S17 Photograph of the home-made three-electrode cell.

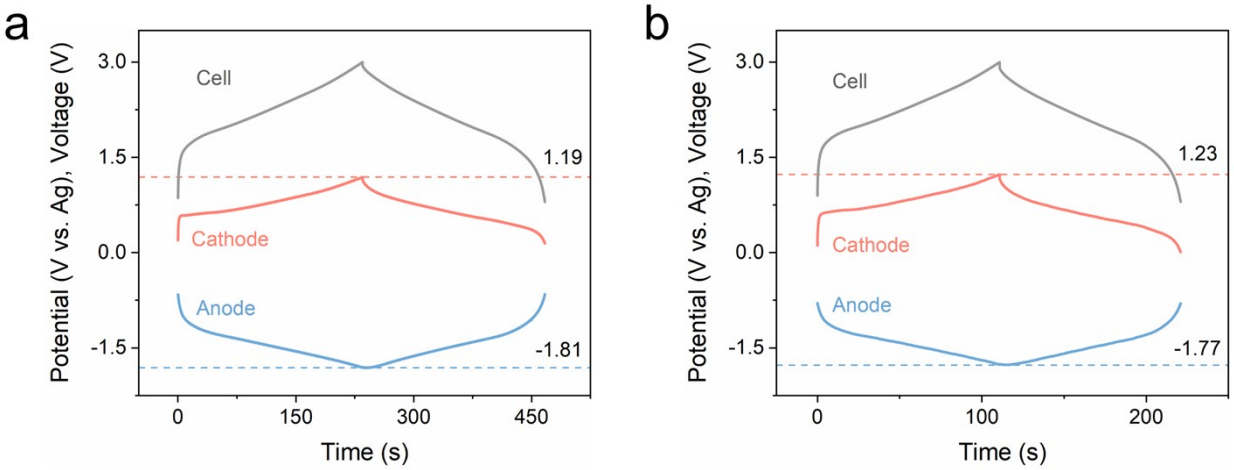

Fig. S18 Potential profiles of the anode, cathode and full cell obtained from the three-electrode GCD measurements of T-Nb_2O_5-NF//NCA-3D BSHD at (a) 1 A g^{-1} and (b) 2 A g^{-1}.

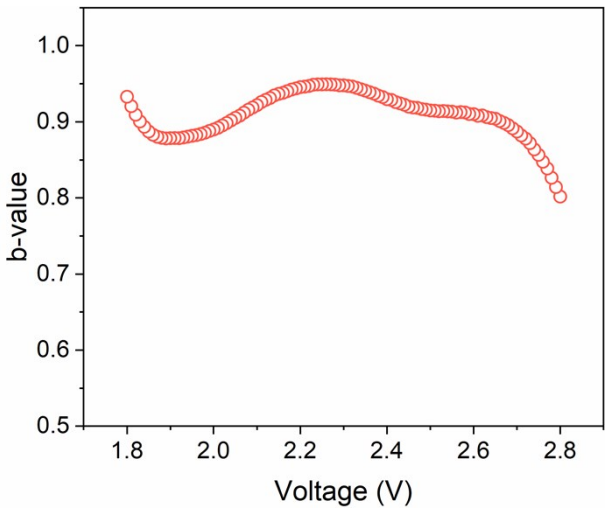

Fig. S19 b-value as a function of voltage for the discharge process of T-Nb_2O_5-NF//NCA-3D BSHD.

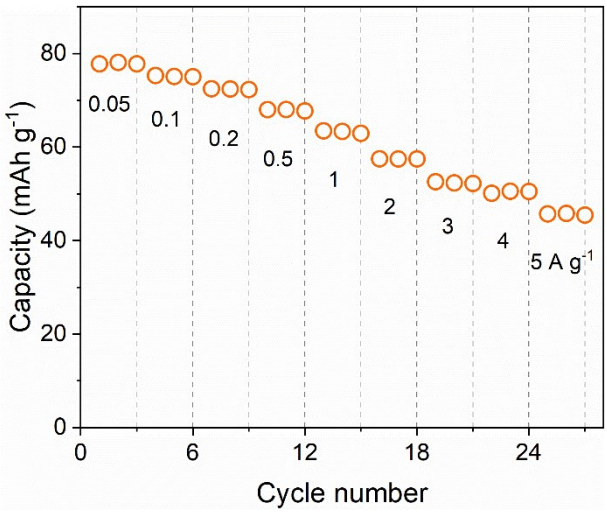

Fig. S20 Rate capability of T-Nb_2O_5-NF//NCA-3D BSHD.

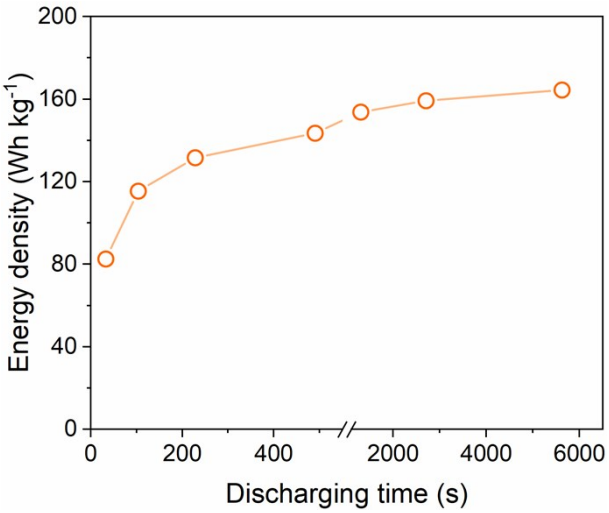

Fig. S21 Energy density of T-Nb_2O_5-NF//NCA-3D BSHD as a function of discharging time.

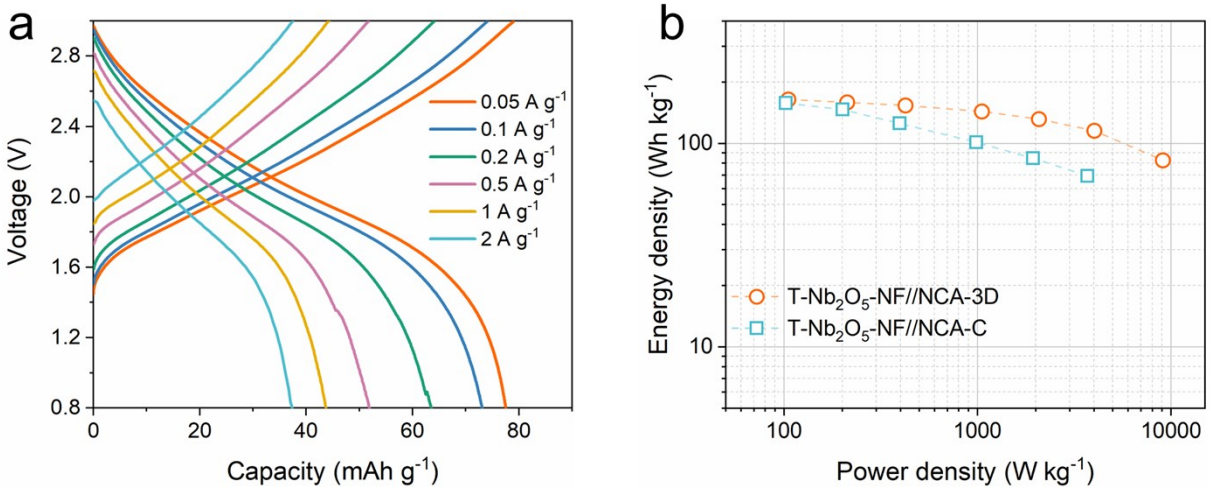

Fig. S22 (a) GCD profiles of T-Nb_2O_5-NF//NCA-C BSHD measured at different current densities. (b) Ragone plots of T-Nb_2O_5-NF//NCA-3D BSHD and T-Nb_2O_5-NF//NCA-C BSHD.

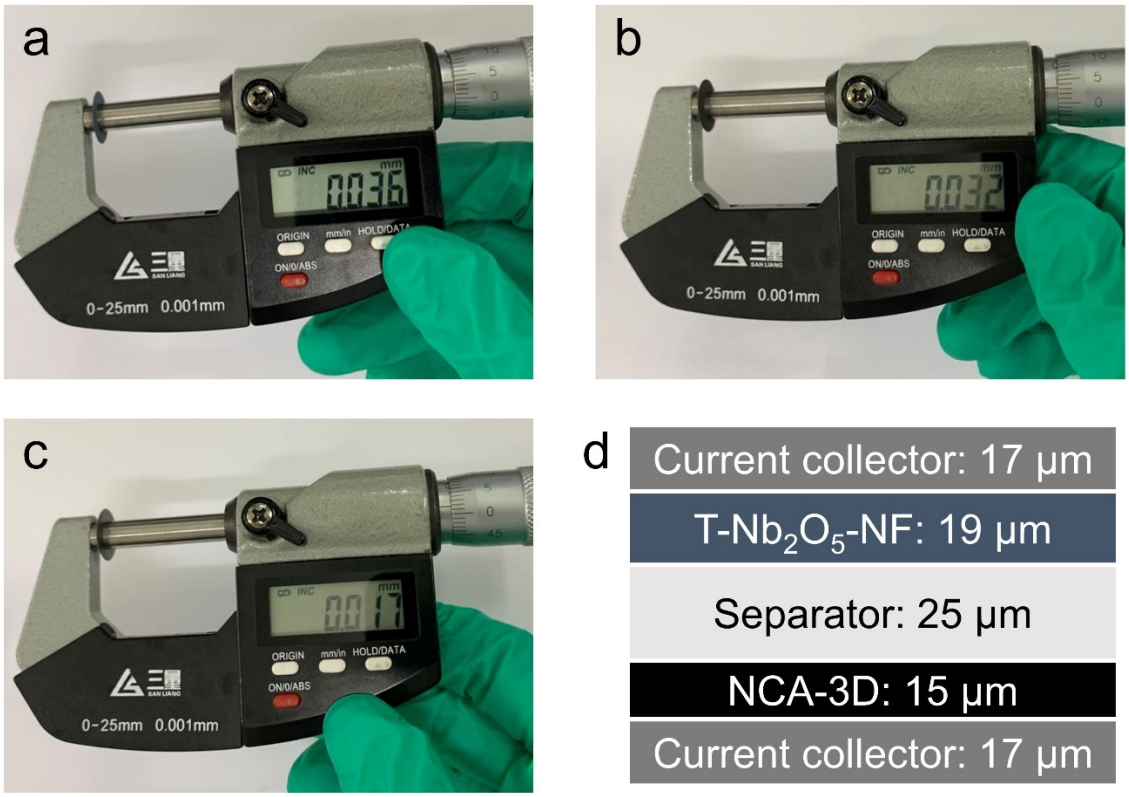

Fig. S23 Thickness measurements of electrode slices for (a) T-Nb_2O_5-NF anode with the total mass loading of 1.75 mg cm^{-2}, (b) NCA-3D cathode with the total mass loading of 1.58 mg cm^{-2} and c) carbon-coated Al foil. (d) Illustration of the configuration of the BSHD full cell.

Supplementary Tables

Table S1 Comparison of T-Nb_2O_5-NF with the previously reported Nb-based oxides.

Active material	Active material: conductive additive:binder	Mass loading (mg cm^{-2})	Rate capability			Ref.
T-Nb_2O_5 nanoflower	80:10:10	1.2-2	100%, 1C	~90%, 5C	~75%, 25C	This work
Triple-shelled Nb_2O_5	70:20:10	1-1.5	100%, 1C	~90%, 5C	~77%, 20C	[8]
Hollow and mesoporous Nb_2O_5 nanospheres	70:20:10	1-1.5	100%, 1C	~90%, 5C	~77%, 25C	[9]
Nitrogen-doped T-Nb_2O_5/tubular carbon	85:5:10	--	100%, 1C	~44%, 10C		[10]
Nb_2O_5@carbon core-shell nanocrystals	80:10:10	0.9-1.1	100%, 1C	~75%, 5C	~52%, 25C	[11]
Macroporous T-Nb_2O_5	70:20:10	--	100%, 1C	~75%, 5C	~56%, 20C	[12]
Nb_2O_5 nanorod film	Free-standing	1.5-2	100%, 1C	~85%, 5C	~73%, 20C	[13]
$Ti_2Nb_{10}O_{29-x}$@C	80:10:10	2	100%, 1C	~84%, 5C	~66%, 20C	[14]
$V_3Nb_{17}O_{50}$ submicron-sized rods	65:25:10	--	100%, 1C	~76%, 5C	~65%, 10C	[15]
$Nb_{12}O_{29}$ hierarchical microspheres	65:25:10	1.4	100%, 1C	~80%, 5C	~69%, 10C	[16]

Table S2 Comparison of NCA-3D with the previously reported nickel-rich layer oxide cathodes.

Cathode material	Current ($A\ g^{-1}$)	Capacity ($mAh\ g^{-i}$)	Current ($A\ g^{-1}$)	Capacity ($mAh\ g^{-i}$)	Ref.
$LiNi_{0.8}Co_{0.15}Al_{0.05}O_2$ with 3D interconnected conductive network	0.05	176	5	116	This work
$LiNi_{0.815}Co_{0.15}Al_{0.035}O_2$@rGO hybrids	0.038	196	0.95	127	[17]
$LiNi_{0.8}Co_{0.15}Al_{0.05}O_2$-graphene composite	0.0556	185	5.56	112	[18]
$FePO_4$ coated $LiNi_{0.8}Co_{0.15}Al_{0.05}O_2$	0.04	180	1	128	[19]
P3HT coated $LiNi_{0.8}Co_{0.15}Al_{0.05}O_2$	0.16	156	5.12	83	[20]
Li_3VO_4-PPy coated $LiNi_{0.6}Co_{0.2}Mn_{0.2}O_2$	0.09	186	1.8	131	[21]
rGO wrapped $LiNi_{0.6}Co_{0.2}Mn_{0.2}O_2$	0.02	183	2	133	[22]
Concentration-gradient $LiNi_{0.7}Co_{0.15}Mn_{0.15}O_2$	0.02	200	4	130	[23]
Li_3PO_4-graphene coated $LiNi_{0.8}Co_{0.1}Mn_{0.1}O_2$	0.04	185	4	85	[24]
CeO_2 modified $LiNi_{0.8}Co_{0.1}Mn_{0.1}O_2$	0.1	180.4	2	152.1	[25]

Table S3 Comparison of T-Nb_2O_5-NF//NCA-3D BSHD with the previously reported BSHDs.

Configuration	Working mechanism	Energy density (Wh kg^{-1}) @ power density (W kg^{-1})		Ref.
T-Nb_2O_5-NF//NCA-3D	Rocking-chair	165@105	83@9100	This work
AC//$LiNi_{0.5}Mn_{1.5}O_4$	Rocking-chair	65@120	40@2000	[26]
MXene//$LiFePO_4$	Rocking-chair	43@11	13@170	[27]
AC//$Li(Mn_{1/3}Ni_{1/3}Fe_{1/3})O_2$-PANI	Rocking-chair	49@1000	18@3000	[28]
MXene//$LiNi_{1/3}Co_{1/3}Mn_{1/3}O_2$	Rocking-chair	160@220		[29]
AC// LFV-GC	Rocking-chair	125.76@108.6	3.36@77	[30]
Nb_2O_5 nanorod//AC	Electrolyte-consuming	95.55@191	65.39@5350.9	[13]
Triple-shelled Nb_2O_5//AC	Electrolyte-consuming	93.8@112.5	19.6@22500	[8]
rGO@VO_2//AC@CC	Electrolyte-consuming	126.7@70	15.2@10000	[31]
CTAB-Sn@Ti_3C_2//AC	Electrolyte-consuming	105.56@495	45.31@10800	[32]
TiC//PHPNC	Electrolyte-consuming	101.5@450	23.4@67500	[33]

References

1. H. Huang, F. Zhou, P. Lu, X. Li, P. Das, X. Feng, K. Muellen and Z.-S. Wu, *Energy Storage Mater.*, 2020, **27**, 396-404.
2. J. P. Zheng, *J. Electrochem. Soc.*, 2003, **150**, A484-A492.
3. Q. Xia, H. Yang, M. Wang, M. Yang, Q. Guo, L. Wan, H. Xia and Y. Yu, *Adv. Energy Mater.*, 2017, **7**, 1701336.
4. G. Li, Z. Yang, Z. Yin, H. Guo, Z. Wang, G. Yan, Y. Liu, L. Li and J. Wang, *J. Mater. Chem. A*, 2019, **7**, 15541-15563.
5. J. P. Zheng, *J. Electrochem. Soc.*, 2005, **152**, A1864-A1869.
6. J. P. Zheng, *J. Electrochem. Soc.*, 2009, **156**, A500-A505.
7. B. Delattre, R. Amin, J. Sander, J. De Coninck, A. P. Tomsia and Y. M. Chiang, *J. Electrochem. Soc.*, 2018, **165**, A388-A395.
8. R. Bi, N. Xu, H. Ren, N. Yang, Y. Sun, A. Cao, R. Yu and D. Wang, *Angew. Chem. Int. Ed.*, 2020, **59**, 4865-4868.
9. Y.-G. Sun, J.-Y. Piao, L.-L. Hu, D.-S. Bin, X.-J. Lin, S.-Y. Duan, A.-M. Cao and L.-J. Wan, *J. Am. Chem. Soc.*, 2018, **140**, 9070-9073.
10. S. Hemmati, G. Li, X. Wang, Y. Ding, Y. Pei, A. Yu and Z. Chen, *Nano Energy*, 2019, **56**, 118-126.
11. E. Lim, C. Jo, H. Kim, M.-H. Kim, Y. Mun, J. Chun, Y. Ye, J. Hwang, K.-S. Ha, K. C. Roh, K. Kang, S. Yoon and J. Lee, *ACS Nano*, 2015, **9**, 7497-7505.
12. S. Lou, X. Cheng, L. Wang, J. Gao, Q. Li, Y. Ma, Y. Gao, P. Zuo, C. Du and G. Yin, *J. Power Sources*, 2017, **361**, 80-86.
13. B. Deng, T. Lei, W. Zhu, L. Xiao and J. Liu, *Adv. Funct. Mater.*, 2018, **28**, 1704330.
14. S. Deng, H. Zhu, G. Wang, M. Luo, S. Shen, C. Ai, L. Yang, S. Lin, Q. Zhang, L. Gu, B. Liu, Y. Zhang, Q. Liu, G. Pan, Q. Xiong, X. Wang, X. Xia and J. Tu, *Nat. Commun.*, 2020, **11**.
15. Q. Fu, X. Zhu, R. Li, G. Liang, L. Luo, Y. Chen, Y. Ding, C. Lin, K. Wang and X. S. Zhao, *Energy Storage Mater.*, 2020, **30**, 401-411.
16. R. Li, X. Zhu, Q. Fu, G. Liang, Y. Chen, L. Luo, M. Dong, Q. Shao, C. Lin, R. Wei and Z. Guo, *Chem. Commun.*, 2019, **55**, 2493-2496.
17. Y. Li, H. Yu, Y. Hu, H. Jiang and C. Li, *J. Energy Chem.*, 2018, **27**, 559-564.
18. S. Yoon, K.-N. Jung, S.-H. Yeon, C. S. Jin and K.-H. Shin, *J. Electroanal. Chem.*, 2012, **683**, 88-93.
19. S. Xia, F. Li, F. Chen and H. Guo, *J. Alloys Compd.*, 2018, **731**, 428-436.
20. C.-H. Lai, D. S. Ashby, T. C. Lin, J. Lau, A. Dawson, S. H. Tolbert and B. S. Dunn, *Chem. Mater.*, 2018, **30**, 2589-2599.
21. Q. Ran, H. Zhao, Y. Hu, Q. Shen, W. Liu, J. Liu, X. Shu, M. Zhang, S. Liu, M. Tan, H. Li and X. Liu, *Electrochim. Acta*, 2018, **289**, 82-93.
22. J.-H. Shim, Y.-M. Kim, M. Park, J. Kim and S. Lee, *ACS Appl. Mater. Interfaces*, 2017, **9**, 18720-18729.
23. P. Hou, F. Li, Y. Sun, H. Li, X. Xu and T. Zhai, *ACS Appl. Mater. Interfaces*, 2018, **10**, 24508-24515.
24. Q. Fan, S. Yang, J. Liu, H. Liu, K. Lin, R. Liu, C. Hong, L. Liu, Y. Chen, K. An, P. Liu, Z. Shi and Y. Yang, *J. Power Sources*, 2019, **421**, 91-99.
25. Y. Ma, F. Lv, Z. Wang, J. Feng, M. Wu, Z. Liu, L. Chen and Y. Gu, *ACS Sustainable Chem. Eng.*, 2020, **8**, 8795-8802.
26. A. Brandt, A. Balducci, U. Rodehorst, S. Menne, M. Winter and A. Bhaskar, *J. Electrochem. Soc.*, 2014, **161**, A1139-A1143.

27. A. Byeon, A. M. Glushenkov, B. Anasori, P. Urbankowski, J. Li, B. W. Byles, B. Blake, K. L. Van Aken, S. Kota, E. Pomerantseva, J. W. Lee, Y. Chen and Y. Gogotsi, *J. Power Sources*, 2016, **326**, 686-694.
28. K. Karthikeyan, S. Amaresh, V. Aravindan, H. Kim, K. S. Kang and Y. S. Lee, *J. Mater. Chem. A*, 2013, **1**, 707-714.
29. S. Kajiyama, L. Szabova, H. Iinuma, A. Sugahara, K. Gotoh, K. Sodeyama, Y. Tateyama, M. Okubo and A. Yamada, *Adv. Energy Mater.*, 2017, **7**, 1601873.
30. Y. Zhang, Z. Zhang, Y. Tang, D. Jia, Y. Huang, W. Pang, Z. Guo and Z. Zhou, *Adv. Funct. Mater.*, 2019, **29**, 1807895.
31. R. Sahoo, T. H. Lee, P. Duy Tho, L. Thi Hoai Thuong and Y. H. Lee, *ACS Nano*, 2019, **13**, 10776-10786.
32. J. Luo, W. Zhang, H. Yuan, C. Jin, L. Zhang, H. Huang, C. Liang, Y. Xia, J. Zhang, Y. Gan and X. Tao, *ACS Nano*, 2017, **11**, 2459-2469.
33. H. Wang, Y. Zhang, H. Ang, Y. Zhang, H. T. Tan, Y. Zhang, Y. Guo, J. B. Franklin, X. L. Wu, M. Srinivasan, H. J. Fan and Q. Yan, *Adv. Funct. Mater.*, 2016, **26**, 3082-3093.